Research Square

Preprints are preliminary reports that have not undergone peer review.
They should not be considered conclusive, used to inform clinical practice,
or referenced by the media as validated information.

$SrZrO_3$-modulated O–T polymorphic phase boundary and improved electromechanical strain in KNNS-BNZ lead-free ceramics

Lizi Chen
Wuhan University of Technology
Yunbing Jiang
Wuhan University of Technology
Zhonghua Yao
yaozhhua@whut.edu.cn
Wuhan University of Technology
Hua Hao
Wuhan University of Technology
Hanxing Liu
Wuhan University of Technology

Research Article

Keywords: Lead-free piezoceramics, KNN, Orthorhombic-tetragonal phase boundary

Posted Date: November 12th, 2026

DOI: https://doi.org/10.21203/rs.3.rs-11386087/v1

License: This work is licensed under a Creative Commons Attribution 4.0 International License.
Read Full License

Additional Declarations: No competing interests reported.

$SrZrO_3$-modulated O–T polymorphic phase boundary and improved electromechanical strain in KNNS-BNZ lead-free ceramics

Lizi Chen[1], Yunbing Jiang[1], Zhonghua Yao[1, 2]*, Hua Hao[1,2], Hanxing Liu[1,2]

[1]State Key Laboratory of Silicate Materials for Architectures, School of Material Science and Engineering, Wuhan University of Technology, Wuhan 430070, China

[2]Sanya Science and Education Innovation Park of Wuhan University of Technology, Sanya, 572000, China

*Corresponding author:

*Zhonghua Yao, E-mail: yaozhhua@whut.edu.cn

Abstract

Lead-free potassium-sodium niobate-based piezoceramics have attracted extensive attention owing to their excellent piezoelectric performance and environment-friendly characteristics. The effects of $SrZrO_3$(SZ) doping content on the phase structure, microstructure, dielectric, ferroelectric, strain and piezoelectric properties of $(0.96\text{-}x)(K_{0.48}Na_{0.52})_{0.96}Li_{0.04}Nb_{0.96}Sb_{0.04}O_3\text{-}0.04Bi_{0.5}Na_{0.5}ZrO_3\text{-}xSrZrO_3$ (KNNS-BNZ-xSZ) ceramics were systematically investigated. X-ray diffraction confirmed pure perovskite phase in all samples, with SZ doping inducing an orthorhombic-tetragonal (O-T) phase transition. SEM observations revealed gradual grain-size reduction upon increasing SZ content, whereas excessive doping degraded ceramic densification. Dielectric-temperature measurements showed a downward shift in Curie temperature after SZ modification. Benefiting from O-T phase coexistence, the x=0.015 ceramic exhibited optimal overall electrical properties: piezoelectric coefficient d_{33}=303 pC/N, planar electromechanical coupling factor k_p=0.39, mechanical quality factor Q_m=65, room-temperature relative permittivity of 2183, Curie temperature T_C=235 ℃, remnant polarization P_r=14.7 μC/cm^2, and a large unipolar strain of 0.12%. This work provides an effective reference for performance optimization of KNN-based lead-free piezoceramics.

Keywords: Lead-free piezoceramics; KNN; Orthorhombic-tetragonal phase boundary

1. Introduction

Lead-zirconate-titanate (PZT)-based piezoelectric ceramics possess excellent electromechanical performance and have been widely applied in actuators, sensors and transducers (*1–5*). Benefiting from their ultra-high piezoelectric coefficient, stable electromechanical coupling performance and mature preparation process, PZT ceramics have long dominated the commercial piezoelectric material market and are indispensable core materials in precision machinery, intelligent sensing, aerospace and micro-electronic devices. Nevertheless, the high content of toxic lead element brings severe environmental and health concerns, which motivates the continuous exploration of lead-free piezoelectric alternatives (*6–8*). With the increasingly stringent global environmental protection regulations and the continuous upgrading of green manufacturing standards, the research and industrialization of high-performance lead-free piezoelectric materials have become an inevitable development trend in the field of functional ceramics, aiming to replace traditional lead-based piezoelectric materials and eliminate lead-pollution risks across the full lifecycle of material preparation, device operation and waste recycling. Among various lead-free systems, potassium-sodium niobate (KNN)-based ceramics are regarded as one of the most promising candidates owing to their relatively high Curie temperature and outstanding piezoelectric potential(*9–15*).

However, pure KNN ceramics suffer from poor sintering activity and unsatisfactory piezoelectric properties (*16–18*). Pure KNN ceramics are prone to volatilization of alkali metal elements during high-temperature sintering, resulting in

low ceramic densification, abundant internal pores and defective grain boundaries. These inherent defects seriously reduce the dielectric, ferroelectric and piezoelectric properties of pure KNN ceramics, greatly limiting their practical engineering application value(*19*, *20*). Chemical modification, including ion substitution and composite doping, has been proven to be an effective strategy to optimize the overall performances of KNN-based ceramics(*21–23*). Constructing polymorphic phase boundary (PPB) near room-temperature, especially orthorhombic-tetragonal (O-T) phase coexistence, can greatly reduce the energy barrier for domain rotation and domain-wall motion, thus improving piezoelectric response(*24–26*). Wu et al. constructed rhombohedral-tetragonal (R-T) polymorphic phase boundary in Bi-Zr modified KNN-Sb-Li ceramics, and a giant piezoelectric coefficient of 490 pC/N was achieved by conventional solid-state sintering, demonstrating the great potential of Bi-Zr-containing dopants for optimizing KNN-based performances(*27*). Further work reported by Liu *et al.* demonstrated that R-O-T tri-phase co-existence induced by $BaZrO_3$ doping produced adaptive ferroelectric states with 63 nm nanodomains, yielding outstanding properties of d_{33}=585 pC/N and k_p=0.62(*28*). Numerous studies have reported that Zr-containing dopants can effectively tailor phase structure, adjust phase transition temperature and enhance electrical properties for KNN-based materials(*29–31*).

$SrZrO_3$ (SZ) is an attractive modifier for niobate perovskite ceramics, but the influences of SZ doping on phase evolution, microstructure and comprehensive electrical behaviors of Bi-modified KNN system still require further investigation(*32*).

Recently, Qi et al. reported KNNS-BNZ-SZ ceramics but only investigated one fixed SZ doping concentration without compositional gradient research(*33*). In this work, a series of SZ-modified KNN-BNZ lead-free piezoceramics were prepared by conventional solid-state reaction. The effects of SZ doping content on crystal structure, grain morphology, dielectric, ferroelectric and piezoelectric properties were systematically studied. Special attention was paid to the regulation of orthorhombic-tetragonal phase boundary as well as the correlation between microstructure and macroscopic electrical performances(*34*). This work is expected to provide experimental basis for developing high-performance KNN-based lead-free piezoelectric ceramics.

2. Experimental

$(0.96\text{-}x)(K_{0.48}Na_{0.52})_{0.96}Li_{0.04}Nb_{0.96}Sb_{0.04}O_3\text{-}0.04Bi_{0.5}Na_{0.5}ZrO_3\text{-}xSrZrO_3$ lead-free piezoelectric ceramics were fabricated by conventional solid-state reaction method. Raw materials including K_2CO_3(99.8%), Na_2CO_3(99.8%), Li_2CO_3(99%), Nb_2O_5(99.9%), Sb_2O_3(99.9%), Bi_2O_3(99%), ZrO_2(99%), $SrCO_3$(99.9%), with analytical purity were weighed according to stoichiometric ratio. The powder was mixed with ethanol and ball milled in a planetary ball mill for 12 h. After drying, the mixed powder was calcined at 850 ℃ for 6 h to synthesize perovskite precursor powder. The calcined powder was ball milled again for 10 h, dried and mixed with 5 wt% PVA binder. The powder was pressed into green pellets with a diameter of 12 mm under uniaxial pressure. The green pellets were first debinded at 600 °C for 2 h, and then sintered at 1080-1120 °C for 3 h in air atmosphere.

For electrical testing, silver paste was coated on both sides of sintered ceramics and sintered at 800 ℃ to form electrodes. The samples were polarized in silicone oil under a direct-current electric field at an appropriate temperature. X-ray diffraction was used to characterize crystal structure. Scanning electron microscopy (SEM) was employed to observe surface microstructure. Room-temperature dielectric constant and dielectric loss were measured by an LCR meter. Dielectric temperature spectra were tested from room temperature to 400 ℃ at 1 kHz. Ferroelectric hysteresis loops (P-E), strain-electric field (S-E) curves were measured by a ferroelectric test system. Piezoelectric constant d_{33} was tested by a quasi-static d_{33} tester; planar electromechanical coupling coefficient k_p and mechanical quality factor Q_m were calculated via resonance-antiresonance method.

3. Results and discussion

Figure 1 displays the XRD patterns of KNN-BNZ-*x*SZ ceramics with different doping concentrations. All samples exhibit typical perovskite diffraction peaks without obvious impurity phase, indicating that BNZ-SZ dopants have successfully diffused into the KNN crystal lattice and formed a single solid solution. The enlarged view around 2θ=43°-47° is presented in Fig. 1(b), which reflects the crystal-structure evolution between orthorhombic (O) and tetragonal (T) phases.

For the undoped sample x=0, two well-separated diffraction peaks can be observed in this region, which is the characteristic feature of orthorhombic (O) phase. As the x increases, the double peaks gradually merge into a single broad peak. This phenomenon demonstrates that SZ doping induces the phase transition from orthorhombic phase

toward tetragonal phase. With increasing SZ content, the fraction of tetragonal phase increases, and the O-T phase boundary shifts toward room temperature. The coexistence of orthorhombic-tetragonal phases appears at moderate doping levels, promoting the piezoelectric performance of KNN-based ceramics. At higher *x* values, the feature of tetragonal phase becomes more prominent. The composition-driven O–T phase evolution reshapes the free-energy landscape and shifts the polymorphic phase boundary toward room temperature, which is an effective strategy to regulate the phase structure of KNN-based ceramics(*35*).

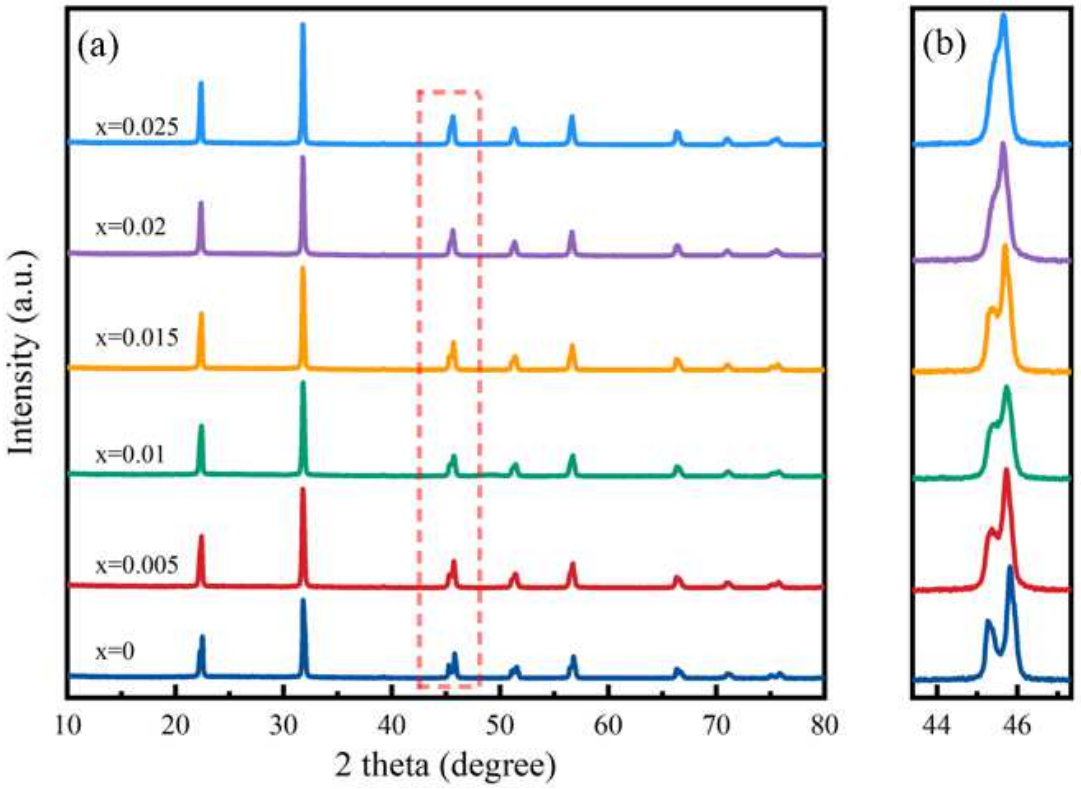


Fig. 1. (a) XRD patterns of the KNNS-BNZ-*x*SZ ceramics with different *x* values; (b) expanded XRD patterns in the 2θ range of 43.5°–47.2° of key peaks in the KNNS-BNZ-*x*SZ ceramics.

Figure 2 shows the SEM micrographs of thermally-etched fractured surfaces for KNNS-BNZ-*x*SZ ceramics with different SZ doping contents. Appropriate SZ doping

can adjust surface diffusion energy, reduce the grain size and improve sintering density. Excessive doping introduces lattice defects, hinders mass transport during sintering, resulting in pore generation and poor densification. The difference in microstructure directly affects macroscopic electrical properties: high-density ceramics possess fewer defects, which is conducive to polarization and reduces leakage current. Since grain growth and densification are strongly governed by mass transport and vacancy chemistry during sintering, excessive dopant refines the grain size and deteriorates the density, thereby degrading the overall electrical properties(*36*).

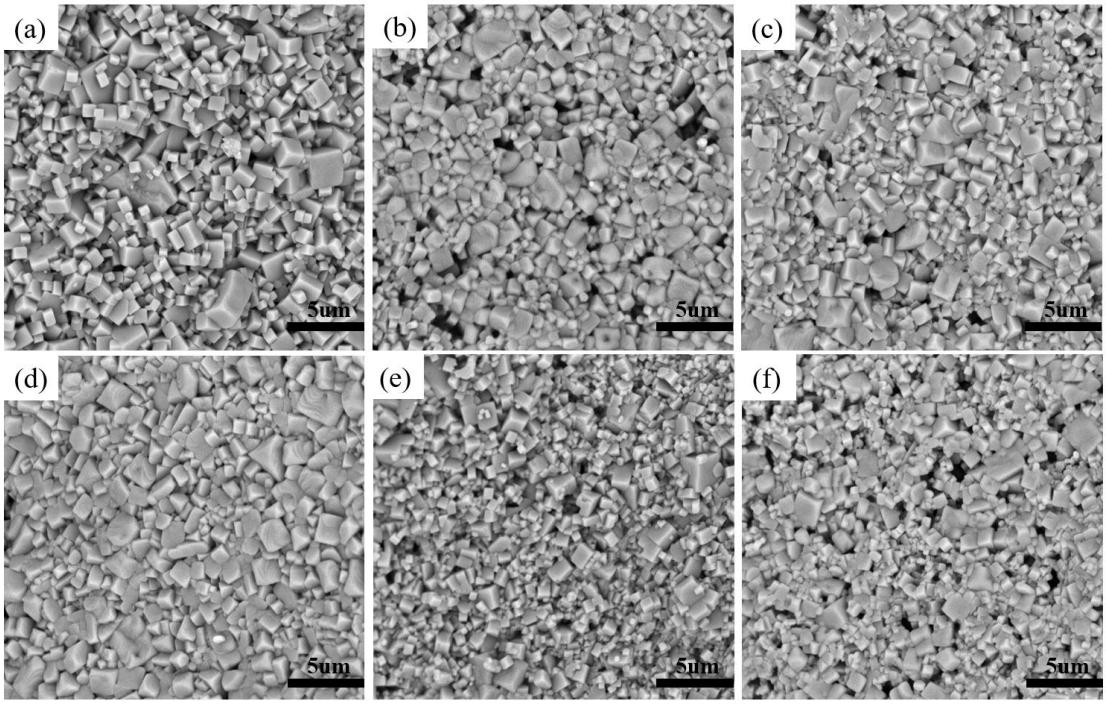


Fig. 2. SEM images of thermally etched fractured surfaces for KNNS-BNZ-*x*SZ samples, (a) *x*=0, (b) *x*=0.005, (c) *x*=0.01, (d) *x*=0.015, (e) *x*=0.02, and (f) *x*=0.025.

Figure 3(a) displays the temperature dependence of relative permittivity and dielectric loss for KNNS-BNZ-*x*SZ ceramics measured upon heating. A prominent dielectric anomaly corresponding to the polymorphic phase transition can be clearly observed for all compositions. As the SZ doping content increases, the dielectric peak

shifts systematically toward lower temperature, demonstrating that SZ incorporation effectively modulates the phase transition temperature of the KNNS-BNZ host lattice. Meanwhile, the maximum permittivity near the phase transition peak first rises and then falls, implying that moderate SZ doping optimizes the polar structural fluctuation in the vicinity of phase boundary.

Notably, all samples maintain relatively low dielectric loss below the phase transition temperature. Upon approaching the transition region, dielectric loss increases distinctly, which is closely associated with the enhanced mobility of domain walls and thermally activated polarization dynamics. At high temperatures beyond the dielectric peak, the sharp growth of dielectric loss is mainly attributed to thermally stimulated space charge conduction and oxygen vacancy migration.

Figure 3(b) summarizes the room-temperature relative permittivity and dielectric loss as a function of x. The room-temperature permittivity increases continuously with rising SZ content and reaches a maximum value at x=0.02, followed by a slight decline at x=0.025. This evolution is consistent with the formation of polymorphic phase boundary (PPB) induced by appropriate ionic substitution. The coexistence of multiple ferroelectric phases provides abundant polarization states, which facilitates domain switching and contributes to improved dielectric response. In contrast, excessive doping disrupts the optimal phase balance and introduces more lattice defects, leading to the degradation of dielectric properties.

The variation trend of room-temperature dielectric loss exhibits mild fluctuation within the investigated doping range. The sample with x=0.02 possesses relatively

higher dielectric loss, which can be explained by enhanced domain wall motion under the PPB environment. Combined with the aforementioned piezoelectric measurements, the evolution of dielectric behavior further verifies that the construction of optimized phase boundary is responsible for the superior electrical performance of KNNS-BNZ-*x*SZ ceramics with moderate SZ doping.

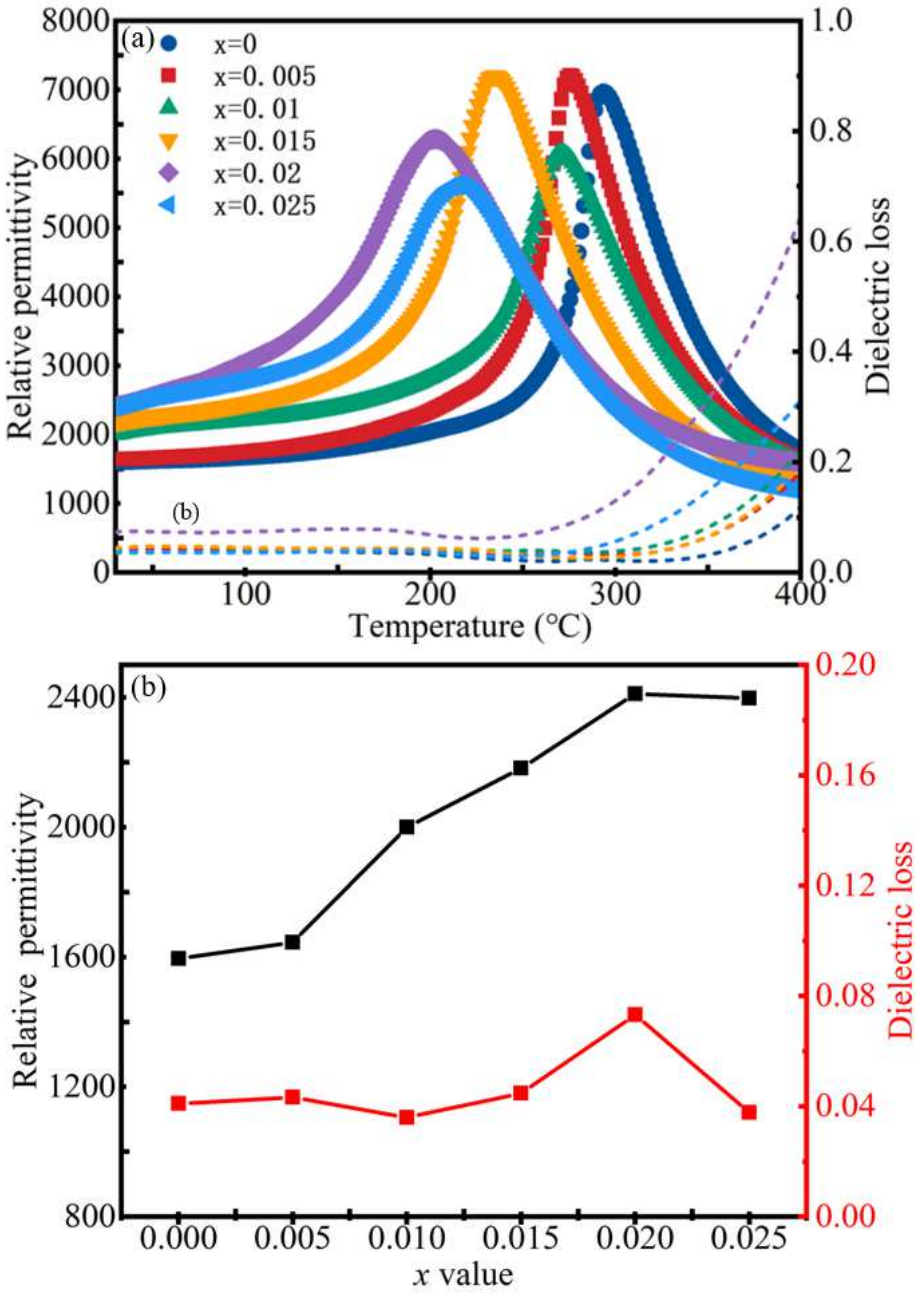


Fig. 3. (a) The dielectric properties versus temperature of the KNNS-BNZ-xSZ

ceramics with different x values; (b) Variations of room-temperature relative permittivity and dielectric loss with x content.

Figure 4(a) illustrates the compositional dependence of piezoelectric coefficient d_{33}, planar electromechanical coupling factor k_p and mechanical quality factor Q_m for KNNS-BNZ-xSZ ceramics measured at room temperature. With increasing SZ doping content, d_{33} and k_p exhibit consistent evolutionary trends, both reaching maximum values at x=0.015. This synchronized variation reveals the intrinsic correlation between piezoelectric activity and electromechanical coupling performance. The optimal piezoelectric response observed at moderate doping level originates from the tailored PPB. The coexistence of multiple ferroelectric phases reduces the energy barrier for polarization rotation and non-180° domain wall motion, which facilitates the generation of large piezoelectric strain under external electric field. When the SZ doping content exceeds x=0.015, excessive ionic substitution breaks the favorable phase equilibrium. The lattice distortion and accumulated defects suppress domain switching dynamics, thus inducing the simultaneous degradation of d_{33} and k_p. Distinctly different from d_{33} and k_p, Q_m gradually drops from x=0 to x=0.015, obtaining the minimum value at x=0.015, and then rises as x further increases to 0.025. At low doping concentrations, the formation of PPB activates abundant domain walls, which enhances piezoelectric activity while introducing extra mechanical loss, leading to Q_m: the continuous reduction of Q_m with rising x. At x=0.015, the optimized phase boundary induces the most active domain wall motion, bringing maximum mechanical loss and the lowest Q_m. Further doping beyond x=0.015 disrupts the multi-phase coexistence state; lattice

defects pin domain walls and restrict their reversible movement, reducing internal friction and resulting in the recovery of Q_m. Such a trade-off between piezoelectric activity and mechanical quality factor is common in phase-boundary-engineered KNN piezoceramics, and can be rationally balanced by embedding local defect dipoles into the O–T phase boundary(*37*).

Figure 4(b) presents the unipolar strain curves of KNNS-BNZ-*x*SZ ceramics under identical applied electric field. The maximum strain amplitude first increases with increasing SZ doping content and reaches its maximum at $x = 0.015$. This evolution trend is similar to the variation of d_{33} and k_p. The x=0.015 sample achieves the largest strain amplitude, indicating that the introduction of SZ facilitates the polarization rotation and domain wall motion under electric field. Nevertheless, the increase of doping concentration also introduces obvious strain hysteresis, which is unfavorable for practical actuator applications.

Combined with the above dielectric characterization results, the evolution of piezoelectric and strain properties unambiguously demonstrates that appropriate SZ doping can effectively modulate the phase structure of KNNS-BNZ matrix and construct a favorable polymorphic phase boundary, which is responsible for the optimized electrical performance of the ceramics. It can be noticed that the enhancement of piezoelectric coefficient d_{33} is relatively limited when comparing the x=0.015 sample with the undoped x=0 composition. Since the base KNNS-BNZ matrix has already been optimized by $Bi_{0.5}Na_{0.5}ZrO_3$ modification, the initial piezoelectric performance of x=0 is already at a relatively high level, which leaves limited room for

further improvement in d_{33} upon subsequent $SrZrO_3$ doping. Nevertheless, the x=0.015 ceramic exhibits several prominent merits other than the moderate increment in d_{33}. A considerable improvement in unipolar strain from 0.10 % (x=0) to 0.12% (x=0.015) is achieved, which is highly desirable for actuator applications. Meanwhile, the room-temperature relative permittivity increases from 1580 to 2183, a feature beneficial for device miniaturization.

Compared with previously reported $SrZrO_3$-modified KNN-based ceramics, the x=0.015 sample achieves a competitive comprehensive performance balance. For instance, similar $SrZrO_3$-doped KNN systems delivered comparable piezoelectric coefficients but exhibited lower Curie temperature(*30*). In the KNNS-BNZ-SZ system reported by Qi et al.(*33*), only one fixed SZ concentration was investigated without compositional optimization; our composition-gradient study further demonstrates that x=0.015 yields improved unipolar strain while maintaining a decent Curie temperature of 235 °C.

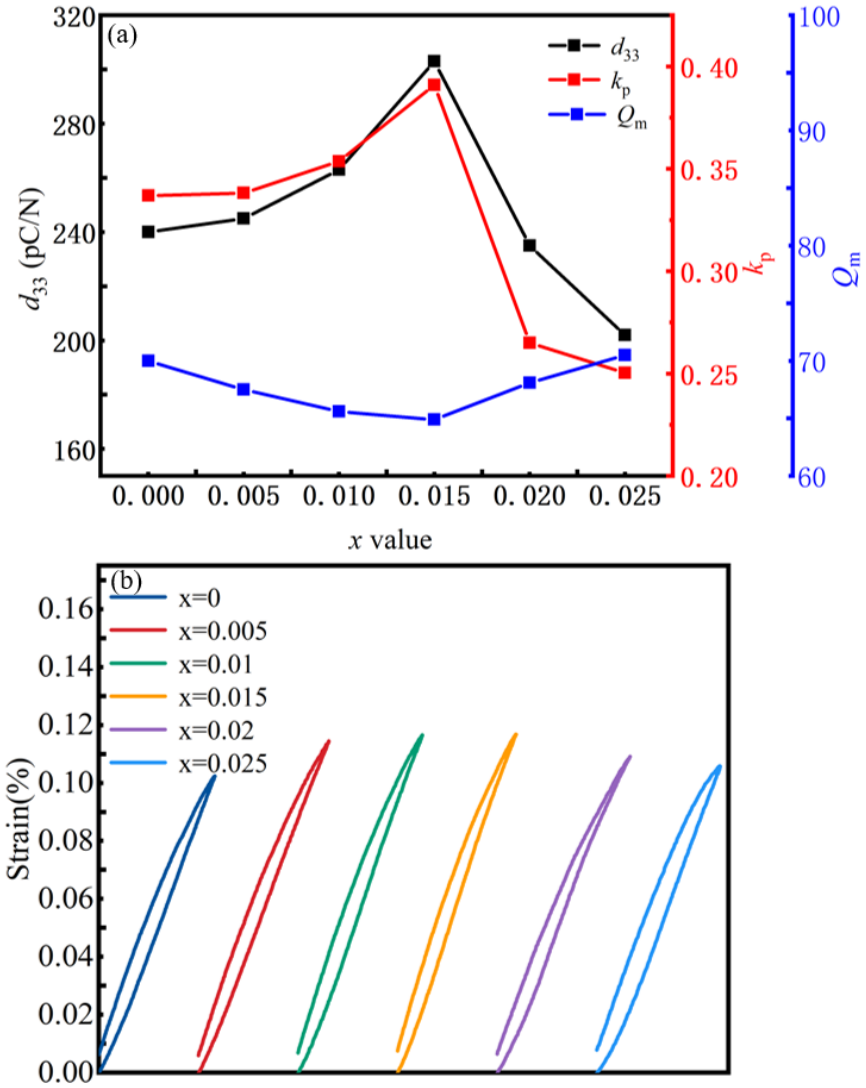


Fig. 4. (a) d_{33}, k_p and Q_m of the KNNS-BNZ-xSZ ceramics as a function of x value; (b) Strain-electric field hysteresis loops of KNNS-BNZ-xSZ ceramics with different x contents.

Figure 5(a) shows the P–E hysteresis loops of KNNS-BNZ-xSZ ceramics measured at room temperature under a maximum electric field of 30 kV/cm. All samples exhibit well-saturated ferroelectric hysteresis curves without obvious leakage distortion, which verifies the good compactness and low leakage conductivity of the sintered ceramics. The extracted remanent polarization P_r and coercive field E_c as functions of SZ doping content are plotted in Figure 5(b).

With increasing x, both P_r and E_c display a continuous decreasing trend. The undoped KNNS-BNZ ceramic possesses relatively high P_r and large E_c, which originates from the single ferroelectric phase with a high energy barrier for domain switching. Moderate SZ substitution induces the formation of PPB with coexisting multiple ferroelectric phases. The flattened free-energy landscape originating from multi-phase coexistence facilitates polarization rotation and activates non-180° domain-wall motion, thus lowering the coercive field E_c. For the x=0.015 sample, E_c is greatly reduced from 1.82 kV/mm to 1.10 kV/mm. A lower coercive field enables domain switching under weaker applied electric fields, facilitates domain alignment during poling and reduces the risk of electrical breakdown for practical industrial fabrication.

Nevertheless, excessive SZ doping introduces considerable lattice disorder and aggravates local polar heterogeneity. The weakened long-range ferroelectric ordering accounts for the gradual decline of remanent polarization P_r. For the sample with x=0.015, the balanced phase structure yields favorable piezoelectric activity, as demonstrated in the preceding d_{33} and k_p results. Although P_r is not at its maximum value, the lowered E_c enables efficient domain reorientation under applied electric field, ultimately contributing to the optimized electromechanical performance.

Combined with the dielectric and piezoelectric characterization above, the evolution of ferroelectric hysteresis parameters further confirms that appropriate SZ doping modulates the phase constitution of KNNS-BNZ matrix and tailors the domain switching dynamics, which provides fundamental insight into the enhanced electrical

properties of the studied ceramics. Defect dipoles and their interaction with spontaneous polarization further tailor the field-induced polarization and strain behavior, offering additional degrees of freedom to optimize the ferroelectric response(*38*).

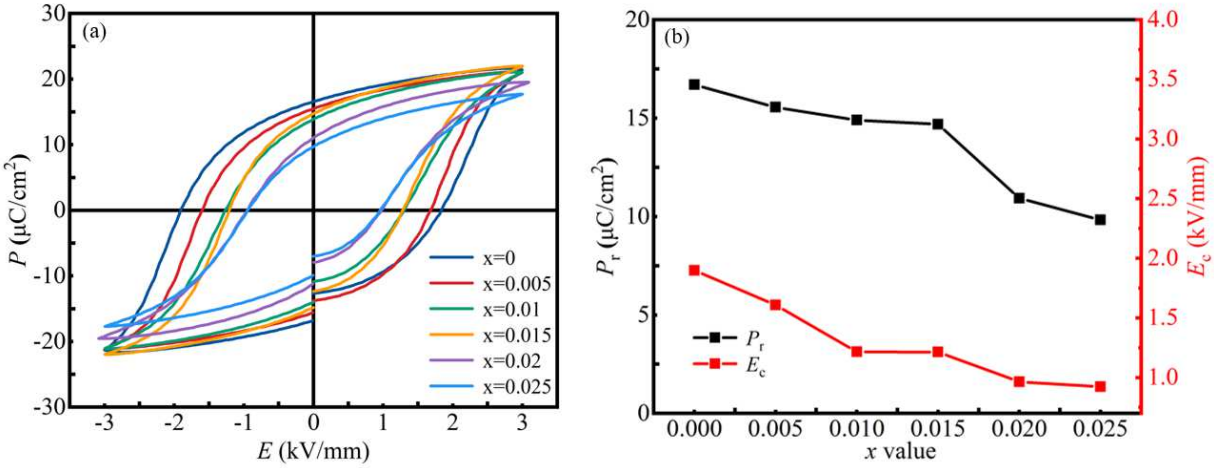


Fig. 5. (a) *P-E* hysteresis loops of ceramics with different *x* contents; (b) P_r and E_c of the ceramics at various *x* values.

Figure 6 presents the temperature dependence of piezoelectric coefficient d_{33} and planar electromechanical coupling factor k_p for the optimized KNNS-BNZ-*x*SZ ceramic (*x*=0.015). In the temperature range from room temperature to approximately 125 °C, both d_{33} and k_p maintain stable and high values without obvious degradation, demonstrating favorable thermal stability of piezoelectric performance within this temperature interval(*39*). As the temperature rises above 125 °C, d_{33} and k_p begin to decrease gradually. With further heating, the two parameters drop sharply and finally approach zero near 250 °C. This remarkable attenuation of piezoelectric activity is closely associated with the ferroelectric-to-paraelectric phase transition across the Curie temperature T_C. Upon approaching T_C, long-range ferroelectric ordering

gradually collapses, and stable ferroelectric domains transform into dynamic polar nanoregions, which drastically suppress the macroscopic piezoelectric response.

d_{33} and k_p exhibit nearly synchronous variation over the whole measured temperature range, which reflects the inherent correlation between piezoelectric strain response and electromechanical coupling effect. The wide temperature window with well-preserved piezoelectric properties confirms that the KNNS-BNZ-*x*SZ ceramics with optimized doping possesses acceptable thermal operating stability, making them suitable for moderate-temperature piezoelectric device applications. Combined with the dielectric-temperature characteristics discussed above, the temperature-induced evolution of piezoelectric parameters is consistent with the dielectric anomaly observed near the phase transition temperature, jointly verifying the thermally activated ferroelectric phase transition behavior of the ceramics.

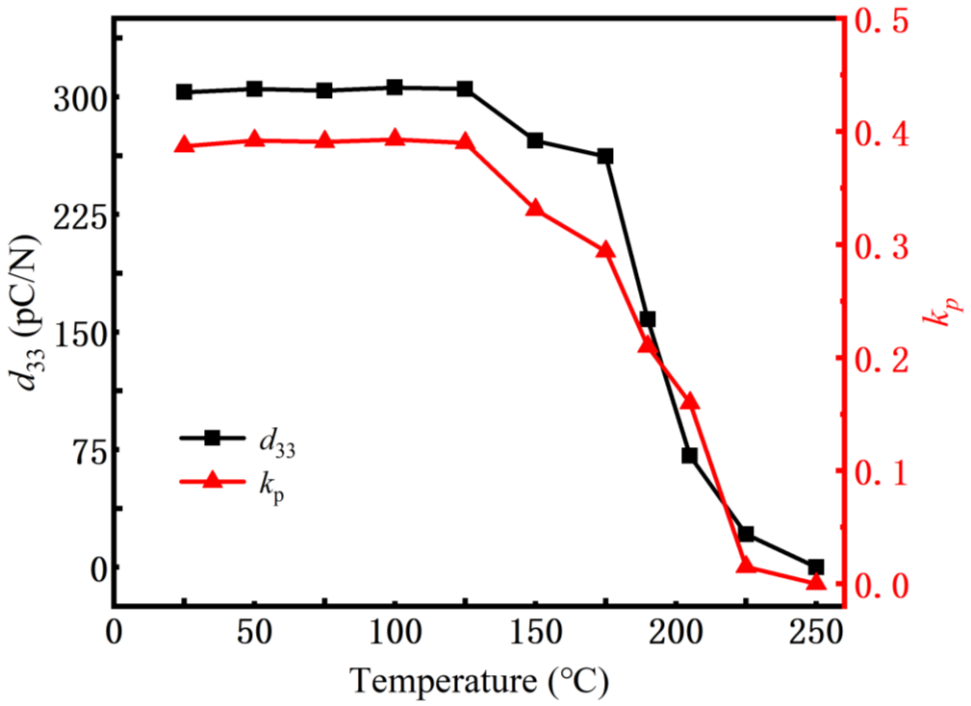


Fig. 6. d_{33} and k_p of the KNNS-BNZ-*x*SZ ceramics with x=0.015 as a function of temperature.

4. Conclusions

In summary, KNN-BNZ-*x*SZ lead-free piezoceramics were synthesized via the conventional solid-state reaction. SZ dopant dissolved into the perovskite lattice without impurity phases and triggers an orthorhombic-tetragonal (O-T) phase transition. SZ addition suppresses grain growth and reduces the Curie temperature T_C, while excessive doping degrades ceramic densification. O-T phase coexistence is realized at moderate SZ content. The x=0.015 sample exhibits optimal comprehensive electrical properties: d_{33}=303 pC/N, k_p=0.39, Q_m=65, room-temperature relative permittivity of 2183, T_C=235 ℃, P_r=14.7 μC/cm^2 and unipolar strain of 0.12%. Further increasing SZ content deteriorates the overall performances due to grain refinement and poor densification. This work demonstrates that SZ modification is an effective strategy to tune phase structure and enhance electrical performances for KNN-based ceramics.

Conflicts of interest

The authors declare that they have no known competing financial interests or personal relationships that could have appeared to influence the work reported in this paper.

Acknowledgements

This work was supported by the National Key Research and Development Program of China (No. 2023YFB3812200), Guangdong Basic and Applied Basic Research Foundation (No. 2026A1515010064), and Natural Science Foundation of China (No. 52472135).

References

1. A. M. M. T. Karim, Y. Liu, J. Daniels, C. Gao, Y. Luo, Z. Cao, X. Liao, Z. Cheng, S. Zhang, Beyond MPB engineering: enhanced piezoelectricity and thermal stability assisted by high-entropy design. *Nat. Commun.* **17**, 6596 (2026).
2. W.-T. Cao, Z. Xu, Z. Zhu, Z. Geng, J.-T. Lu, Z. Zhong, H.-F. Huang, J.-X. Liu, Y. Jiang, Y.-X. Liu, W. Gao, D. Zhu, K. Huang, M. Zheng, K. Bi, K. Wang, High-power performance enhancement in PZT-based piezoceramics via hot-pressing. *Nat. Commun.* **16**, 9778 (2025).
3. M. Waqar, H. Wu, J. Chen, K. Yao, J. Wang, Evolution from Lead-Based to Lead-Free Piezoelectrics: Engineering of Lattices, Domains, Boundaries, and Defects Leading to Giant Response. *Adv. Mater.* **34**, 2106845 (2022).
4. X. Jiang, D. Lu, B. Yin, Z. Leng, Advancing carbon nanomaterials-engineered self-sensing cement composites for structural health monitoring: A state-of-the-art review. *J. Build. Eng.* **87**, 109129 (2024).
5. P. K. Panda, B. Sahoo, PZT to Lead Free Piezo Ceramics: A Review. *Ferroelectrics* **474**, 128–143 (2015).
6. X. Yuan, J. Shi, Y. Kang, J. Dong, Z. Pei, X. Ji, Piezoelectricity, Pyroelectricity, and Ferroelectricity in Biomaterials and Biomedical Applications. *Adv. Mater.* **36**, 2308726 (2024).
7. S. Zhang, B. Malič, J.-F. Li, J. Rödel, Lead-free ferroelectric materials: Prospective applications. *J. Mater. Res.* **36**, 985–995 (2021).
8. J. Rödel, K. G. Webber, R. Dittmer, W. Jo, M. Kimura, D. Damjanovic, Transferring lead-free piezoelectric ceramics into application. *J. Eur. Ceram. Soc.* **35**, 1659–1681 (2015).
9. L. Xu, J. Lin, Y. Yang, Z. Zhao, X. Shi, G. Ge, J. Qian, C. Shi, G. Li, S. Wang, Y. Zhang, P.

Li, B. Shen, Z. Fu, H. Wu, H. Huang, F. Li, X. Ding, J. Sun, J. Zhai, Ultrahigh thermal stability and piezoelectricity of lead-free KNN-based texture piezoceramics. *Nat. Commun.* **15**, 9018 (2024).

10. G.-S. Lee, J.-S. Kim, S.-H. Kim, S. Kwak, B. Kim, I.-S. Kim, S. Nahm, Recent Developments in (K, Na)NbO_3-Based Lead-Free Piezoceramics. *Micromachines* **15**, 325 (2024).

11. K. Zheng, N. Xie, Y. Deng, M. Febbo, C. Broeckmann, P. Liu, A review on lead-free piezoelectric ceramic sensors for sustainable and intelligent applications. *Chem. Eng. J.* **528**, 172363 (2026).

12. H. Xue, X. Huang, X. Sun, K. Wu, Z. Tan, H. Fan, J. Sun, L. Jiang, J. Wu, Superior lead-free piezoceramics for wearable multimodal ultrasound imaging arrays. *Nat. Commun.* **17**, 218 (2025).

13. C.-B.-W. Li, Z. Li, J. Wang, Y.-X. Liu, J.-T. Lu, Z. Xu, P.-S. Soon, K. Bi, C. Chen, K. Wang, Sodium lithium niobate lead-free piezoceramics for high-power applications: Fundamental, progress, and perspective. *J. Adv. Ceram.* **12**, 1–23 (2023).

14. C. Shi, J. Ma, J. Wu, X. Wang, F. Miao, Y. Huang, K. Chen, W. Wu, B. Wu, Coexistence of excellent piezoelectric performance and high Curie temperature in KNN-based lead-free piezoelectric ceramics. *J. Alloys Compd.* **846**, 156245 (2020).

15. S. Mondal, S. Poddar, S. Bhattacharjee, S. Maiti, A. Banerjee, K. K. Chattopadhyay, Lead free halide perovskite embedded PVDF based efficient mechanical energy harvester: Self-driven respiratory sensor. *Nano Energy* **115**, 108689 (2023).

16. M. Bah, R. Podor, R. Retoux, F. Delorme, K. Nadaud, F. Giovannelli, I. Monot-Laffez, A. Ayral, Real-Time Capturing of Microscale Events Controlling the Sintering of Lead-Free

Piezoelectric Potassium-Sodium Niobate. *Small* **18**, 2106825 (2022).

17. B. Malič, J. Koruza, J. Hreščak, J. Bernard, K. Wang, J. Fisher, A. Benčan, Sintering of Lead-Free Piezoelectric Sodium Potassium Niobate Ceramics. *Materials* **8**, 8117–8146 (2015).

18. W. Yang, P. Li, S. Wu, F. Li, B. Shen, J. Zhai, A Study on the Relationship Between Grain Size and Electrical Properties in (K,Na)NbO_3 -Based Lead-Free Piezoelectric Ceramics. *Adv. Electron. Mater.* **5**, 1900570 (2019).

19. Z. Cen, Z. Dong, Z. Xu, F.-Z. Yao, L. Guo, L. Li, X. Wang, Improving fatigue properties, temperature stability and piezoelectric properties of KNN-based ceramics via sintering in reducing atmosphere. *J. Eur. Ceram. Soc.* **41**, 4462–4472 (2021).

20. J. Tao, Y. Wang, X. Zheng, C. Zhao, X. Jin, W. Wang, T. Lin, A review: Polyacrylonitrile as high-performance piezoelectric materials. *Nano Energy* **118**, 108987 (2023).

21. H. Li, H. Chen, X. Li, J. Xing, W. Liu, Z. Tan, M. Mo, N. Chen, M. Tang, J. Zhu, Hardening Effect on the Electromechanical Properties of KNN-Based Ceramics Using a Composite Approach. *ACS Appl. Mater. Interfaces* **15**, 36576–36586 (2023).

22. Y. Zhang, J.-F. Li, Review of chemical modification on potassium sodium niobate lead-free piezoelectrics. *J. Mater. Chem. C* **7**, 4284–4303 (2019).

23. T. Zheng, Y. Yu, H. Lei, F. Li, S. Zhang, J. Zhu, J. Wu, Compositionally Graded KNN-Based Multilayer Composite with Excellent Piezoelectric Temperature Stability. *Adv. Mater.* **34**, 2109175 (2022).

24. M.-H. Zhang, C. Shen, C. Zhao, M. Dai, F.-Z. Yao, B. Wu, J. Ma, H. Nan, D. Wang, Q. Yuan, L. L. Da Silva, L. Fulanović, A. Schökel, P. Liu, H. Zhang, J.-F. Li, N. Zhang, K. Wang, J. Rödel, M. Hinterstein, Deciphering the phase transition-induced ultrahigh piezoresponse in

(K,Na)NbO_3-based piezoceramics. *Nat. Commun.* **13**, 3434 (2022).

25. A. Song, Y. Liu, T. Feng, H. Li, Y. Zhang, X. Wang, L. Liu, B. Zhang, J. Li, Simultaneous Enhancement of Piezoelectricity and Temperature Stability in KNN-Based Lead-Free Ceramics Via Layered Distribution of Dopants. *Adv. Funct. Mater.* **32**, 2204385 (2022).

26. Y. Cheng, J. Xing, X. Li, L. Xie, Y. Xie, Z. Tan, J. Zhu, Meticulously tailoring phase boundary in KNN-based ceramics to enhance piezoelectricity and temperature stability. *J. Am. Ceram. Soc.* **105**, 5213–5221 (2022).

27. X. Wang, J. Wu, D. Xiao, J. Zhu, X. Cheng, T. Zheng, B. Zhang, X. Lou, X. Wang, Giant Piezoelectricity in Potassium–Sodium Niobate Lead-Free Ceramics. *J. Am. Chem. Soc.* **136**, 2905–2910 (2014).

28. Y. Liu, J. Fan, X. Qi, B. Shen, R. Zhang, K. Yao, Adaptive ferroelectric states in KNN-based piezoceramics: Unveiling the mechanism of enhancing piezoelectric properties through multiple phase boundary engineering. *Nano Energy* **128**, 109972 (2024).

29. C. Shi, J. Ma, J. Wu, K. Chen, B. Wu, $(Bi_{0.5}Na_{0.5})ZrO_3$ modified KNN-based ceramics: Enhanced electrical properties and temperature insensitivity. *Ceram. Int.* **46**, 2798–2804 (2020).

30. J. Zhou, G. Xiang, J. Shen, H. Zhang, Z. Xu, H. Li, P. Ma, W. Chen, Composition-insensitive enhanced piezoelectric properties in $SrZrO_3$ modified (K, Na)NbO_3-based lead-free ceramics. *J. Electroceramics* **44**, 95–103 (2020).

31. R. Zhao, Y. Li, Z. Zheng, W. Kang, Phase structure regulation and enhanced piezoelectric properties of Li-doped KNN-based ceramics. *Mater. Chem. Phys.* **245**, 122806 (2020).

32. B. Yang, Z. Zheng, T. Zhang, J. Guo, Ultra-Low Dielectric Loss and High Depolarization

Temperature Achieved in (K,Na)NbO_3 -Based Piezoceramics via Modulating Carrier Migration and Domain Dynamics. *Adv. Energy Mater.* **16**, e70918 (2026).

33. X. C. Qi, P. R. Ren, X. Q. Tong, X. Wang, F. P. Zhuo, Enhanced piezoelectric properties of KNN-based ceramics by synergistic modulation of phase constitution, grain size and domain configurations. *J. Eur. Ceram. Soc.* **45**, 116874 (2025).

34. Y. Zhang, X. Feng, F. Li, D. Meng, T. Zheng, J. Wu, Grain Boundary Diffusion Hardening in Potassium Sodium Niobate-Based Ceramics with Full Gradient Composition and High Piezoelectricity. *Adv. Funct. Mater.* **33**, 2306039 (2023).

35. S. Gao, P. Li, J. Qu, M. Sun, J. Hao, P. Fu, Z. Pan, J. Zhai, W. Li, Temperature-insensitive KNN-based ceramics by elevating O-T phase transition temperature and crystal texture. *J. Materiomics* **9**, 261–268 (2023).

36. Y.-J. Park, I.-R. Yoo, S.-H. Choi, J. Cho, K.-H. Cho, Grain Growth Behavior and Electrical Properties of $0.96(K_{0.46-x}Na_{0.54-x})Nb_{0.95}Sb_{0.05}O_3–0.04Bi_{0.5}(Na_{0.82}K_{0.18})_{0.5}ZrO_3$ Ceramics. *Materials* **15**, 2357 (2022).

37. X. Qiu, C. Wu, D. Q. Tan, R. Liang, C. Liu, Y. Ma, X. Zhang, S. Wei, J. Zhang, Z. Tan, Z. Wang, X. Lv, J. Wu, Excellent hardening effect in lead-free piezoceramics by embedding local Cu-doped defect dipoles in phase boundary engineering. *Nat. Commun.* **16**, 2894 (2025).

38. S. Tian, B. Wang, B. Li, Y. Guo, S. Zhang, Y. Dai, Defect dipole stretching enables ultrahigh electrostrain. *Sci. Adv.* **10**, eadn2829 (2024).

39. S. Tian, Z. Zhao, B. Li, Y. Dai, Microstructural engineering for temperature-stable piezoresponse in KNN-based lead-free piezoceramics: a comprehensive review. *Microstructures* **6** (2026).